 doi:10.20944/preprints201710.0043.v1

Set-up method on properties of $Ba_xSr_{1-x}TiO_3$ thin films deposited by RF-magnetron co-sputtering by projecting temperature and stoichiometric effect

J. L. Estrada-Martínez[a,c], J. A. Melo-Banda[a], U. Páramo-García[a], J. Reséndiz-Muñoz[c], J. L. Fernández-Muñoz[b]*, M. Meléndez-Lira[c], O. Zelaya-Ángel[c],

[a]Tecnológico Nacional de México, Instituto Tecnológico de Ciudad Madero, Centro de Investigación en Petroquímica Secundaria, Prol. Bahía de Aldhair y av. de las Bahías, parque de la pequeña y mediana industria, Tecno, Altamira, Tamaulipas,

[b]Instituto Politécnico Nacional, Laboratorio de Materiales Funcionales, CICATA-Legaria, Legaria 694 Col. Irrigación, CP. 11500 CDMX, México.

[c]Departamento de Física, CINVESTAV-IPN, Av. Instituto Politécnico Nacional 2508, Gustavo A. Madero, San Pedro Zacatenco, C.P. 07360, CDMX, México.

***Corresponding author:** jlfernandez@ipn.mx

Abstract

Thin films (100-400 nm) of $Ba_xSr_{1-x}TiO_3$ ($0 \leq x \leq 1$) deposited in RF-magnetron co-sputtering equipment are presented in this research work. The change of deposition rate, gap energy, and resistivity as a function of temperature- applied power change in the growth parameters was studied through the ISO colour-code lines constructed with MATLAB:

By analysing the trend information and take into account the influence of the calculated "x" parameter with the Boltzmann profile fitting is proposed a method to allow a controlled set up of the RF-magnetron co-sputtering system and predict the E_g and resistivity values in the $Ba_xSr_{1-x}TiO_3$ solid solution with $0 \leq x \leq 1$ for amorphous and crystalline phases. Also, a versatile tool to optimise the deposition process and material properties.

keywords: $Ba_xSr_{1-x}TiO_3$ films; boltzmann modelling; optical band gap; deposition rate; stoichiometric content

Preprints (www.preprints.org) | NOT PEER-REVIEWED | Posted: 9 October 2017 doi:10.20944/preprints201710.0043.v1

1. Introduction

The solid solution $Ba_XSr_{1-X}TiO_3$ (BST), is a ceramic material with perovskite structure, whose technological applications are extensive in the elaboration of optical devices, resistive memories, solar cells, sensors, etc. [1,2,3]. The deposition rate (DR) and the stoichiometric parameter "x" are influenced by geometric deposition system, the gas pressure and the power applied to each of the magnetrons. From the geometry, the DR follows an exponential growth profile, and the parameter "x" follows a sigmoid profile when the target distance decreases while keeping the gas pressure and the temperature of the reservoir constant. The effects of the stoichiometry defined by the value of the parameters x and 1-x. In the BST chemical formula have been investigated in some physical properties such as resistive switching [5,6], resistivity (RST) in crystalline and amorphous phases[7,8,9], the thickness [10], the gap energy (E_g) [11,12,13]. The E_g as a function of temperature and its effect on the improvement of crystallinity [14,15] and the amorphous to crystalline phase change [16,17,18].

Based on the literature review, the combined effect of the parameter "x" with values of $0 \leq x \leq 1$ in applied power and temperature ranges to predict DR values, E_g and RST, has not been investigated; only DR and RST as a function of the power applied, for different deposition pressures in thin films of molybdenum by means of RF-sputtering [19].

In this manuscript the Boltzmann profile fitts (BP) of the experimental data of parameter "x" were calculated using: a) %atomic measured by BST/Nicromel EDS at 495 °C (BP_{EDS}) [6], b) method of normalization and transformation of the positions of the BST/Quartz diffraction peaks at 549 °C (BP_{DRX}) [10].

Total applied power on targets of $BaTiO_3$ and $SrTiO_3$ for every discrete experimental point is applied power ratio P_{Ba}/P_{Sr} (APR). The “y” axis on ISO colour-code lines (ISO lines: ISO-DR, ISO-E_g, ISO-RST) represent the next APR: 0/120 W, 15/105 W, 30/90 W, 45/75 W, 60/60 W, 75/45 W, 90 / 30 W, 105/15 W and 120/0 W, however, for simplicity only the applied power values on $BaTiO_3$ target are shown.

2. Experimental details

BST films were prepared by RF-magnetron co-sputtering in a system equipped with two magnetrons working simultaneously by different power totalling a total of 120 watts: $BaTiO_3$ (99.95%, SCI Engineered Materials Inc) and $SrTiO_3$ (99.9%, SCI Engineered Materials Inc.). Targets were 2” diameter and 0.125” thick. Before solid film deposition, the sputtering chamber was evacuated to a base pressure around $1.2X10^{-3}$ Pa; then, an Ar flushing was done filling the chamber to a pressure of 3.9 Pa during 10 minutes. For the film substantial deposition, an Ar^+/O_2 gas mixture was introduced into the chamber with an Ar/O_2=90/10 ratio at an initial pressure of 6.6 Pa to ignite the plasma and perform a target pre-sputtering during 15 minutes. After that, the working pressure was set at 3.9 Pa

Preprints (www.preprints.org) | NOT PEER-REVIEWED | Posted: 9 October 2017 doi:10.20944/preprints201710.0043.v1

to carry out the deposition. Quartz substrates 1x1.5 cm^2 were successively rinsed with trichloroethylene, acetone, and ethanol before depositing. A stainless-steel substrate holder was fixed at a distance of 8 cm from the magnetron in off-axis configuration. The substrate holder was rotated at 100 rpm for ensuring film uniformity, and the substrate temperature was set at room temperature (as-deposited), 375°C, 435°C, 495°C and 549°C. The total RF-magnetron applied power was 120 W, distributed between the two magnetrons as shown in Table 1, to produce $Ba_xSr_{1-x}TiO_3$ films with different stoichiometric *compositions.* The sputter time for all of the samples was 68 minutes. Chemical composition was obtained by energy dispersive X-ray spectroscopy (EDS) employing a Jeol JSM-5300 electron microscope equipped with a Kevex Delta 1 spectrometer. The optical transmission spectra of the films were obtained in a Perkin-Elmer, Lambda 40 Spectrophotometer in the range of 250 to 800 nm. Film thicknesses were calculated from the transmittance spectra using the SCOUT software. The X-ray diffractograms were acquired in a Phillips X´Pert diffractometer using CuKα=1.54060 Å.

Temperatures As-deposited, 375°C, 435°C, 495°C, 549°C	**RF-Magnetron applied power (W)**		**Total applied power**
Sample	**$BaTiO_3$**	**$SrTiO_3$**	
B0S120	0	120	120
B15S105	15	105	120
B30S90	30	90	120
B45S75	45	75	120
B60S60	60	60	120
B75S45	75	55	120
B90S30	90	30	120
B105S15	105	15	120
B120S0	120	0	120

Table 1. RF- applied power to $BaTiO_3$ and $SrTiO_3$ targets and deposition temperatures for each sample.

3. Results and discussion

Figure 1 shows the experimental discrete points values of the parameter "x" and “1-x", and the solid lines represent the setting of the BP for each storage temperature. The difference among all of the BP can be explained because of BST/Quartz deposition, there are areas rich in Ba (Ba-rich) and rich in Sr (Sr-rich) due to the substrate effect and plasma geometry into RF-sputtering deposition system,

Preprints (www.preprints.org) | NOT PEER-REVIEWED | Posted: 9 October 2017 doi:10.20944/preprints201710.0043.v1

causing a differentiated distribution in the substrate; see figure 4 in [20]. For example, in $Ba_{0.4}Sr_{0.6}TiO_3$ (Ba/Sr = 2/3) and $Ba_{0.5}Sr_{0.5}TiO_3$ (Ba/Sr = 1) thin films deposited by direct current arc discharge plasma process in the Sr-rich zone, the original Ba/Sr ratio decreases to approximately 1/3 and 2/3 respectively [21].

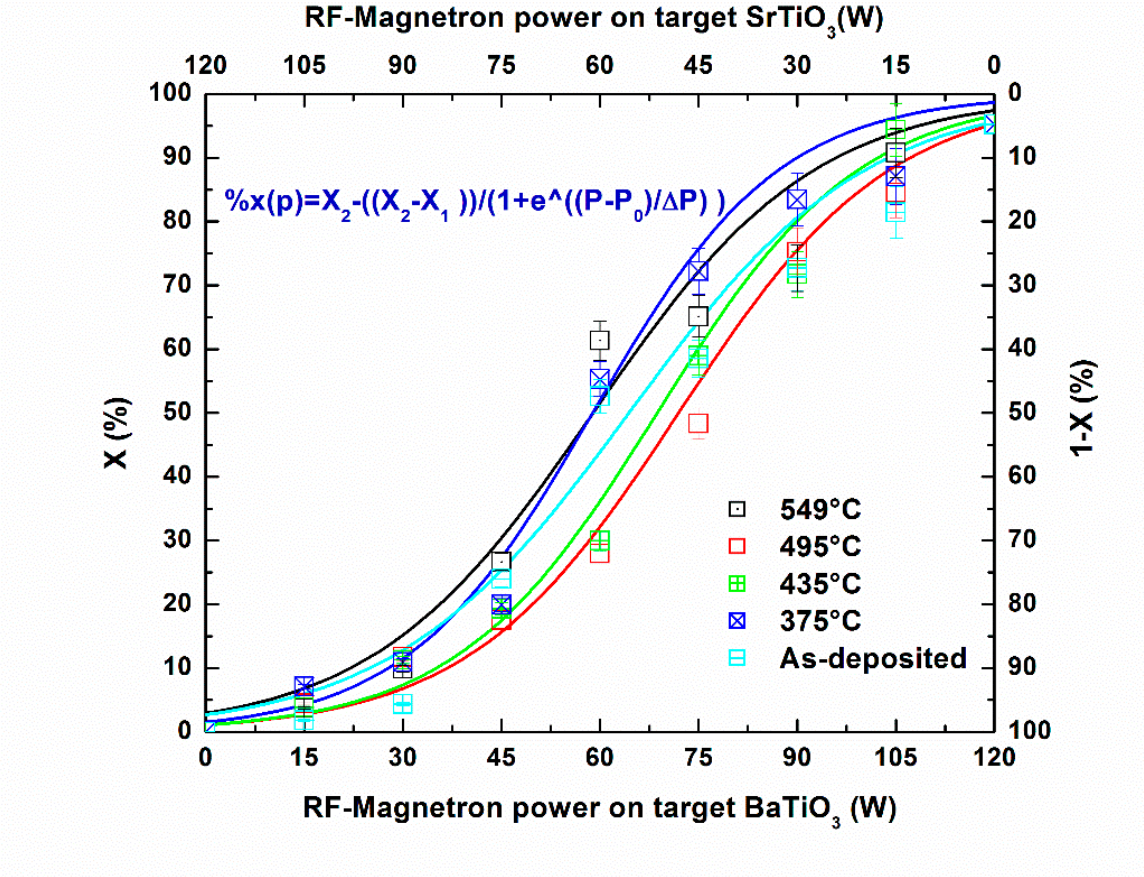

Figure 1. Boltzmann profile of the parameter "x" obtained by EDS and power dependent on the different in-situ deposition temperatures.

Preprints (www.preprints.org) | NOT PEER-REVIEWED | Posted: 9 October 2017 doi:10.20944/preprints201710.0043.v1

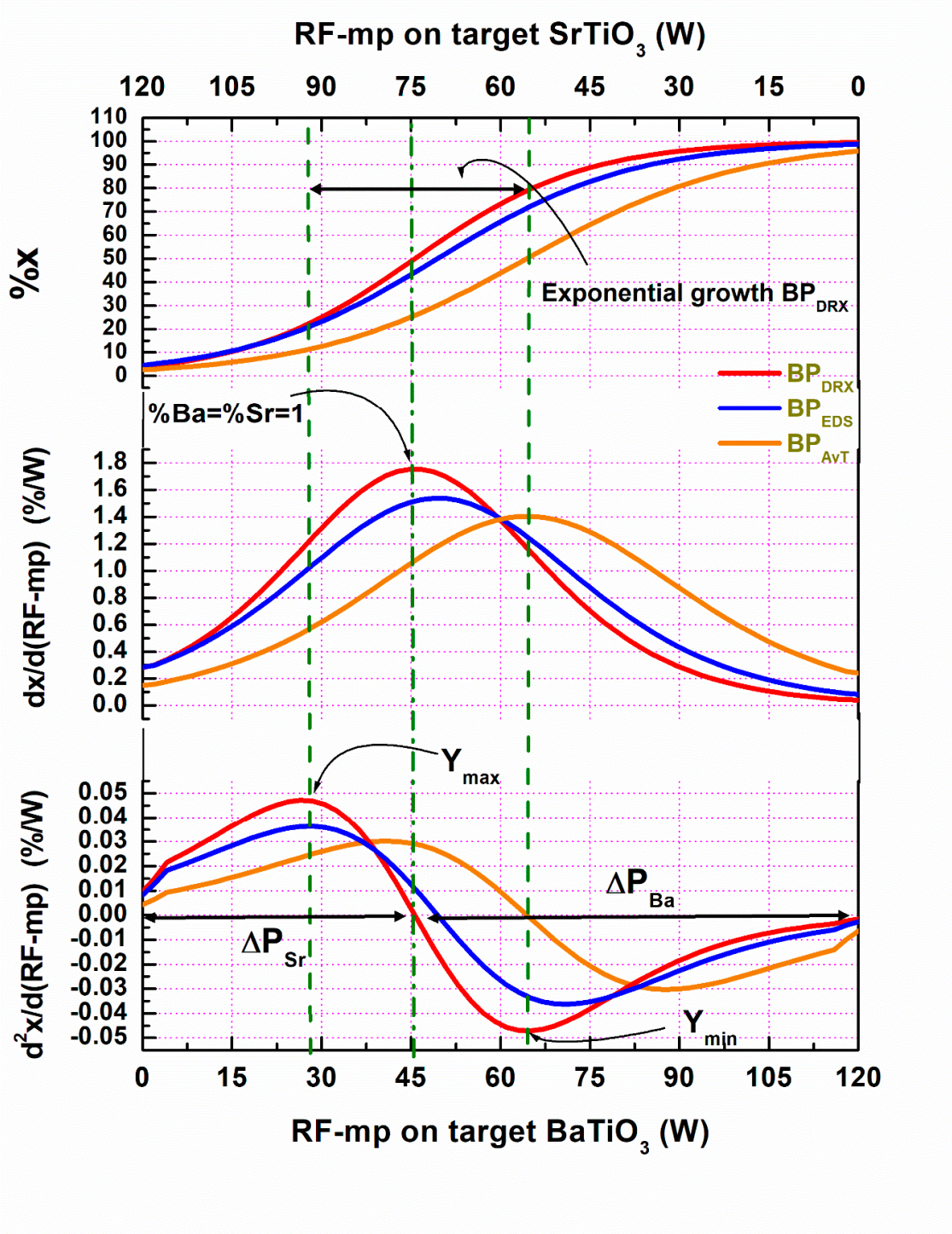

Figure 2. (a) BP_{DRX}, BP_{EDS}, BP_{AvT}, (b) first derivative 2a., (c) second derivative fig. 2a.

Figure 2 (a) shows fit: BP_{DRX}, BP_{EDS} and BP_{AvT} this last one obtained from the experimental values, averaging the fit of parameter "x" from temperatures: as-deposited, 375, 435, 495 and 549 °C. Comparing BP_{EDS} and BP_{AvT}, the effect of the substrate on the Ba/Sr ratio is evident. The

Preprints (www.preprints.org) | NOT PEER-REVIEWED | Posted: 9 October 2017 doi:10.20944/preprints201710.0043.v1

characterization method to calculate the parameter "x" and the storage temperature between BP_{DRX} and BP_{EDS} are different. The area under the curve BP_{DRX}≈3/2.

Therefore, it is defined that the applied power intervals with higher content of Sr and Ba in ISO lines are: 0-45 W and 45-120 W, respectively

However, the fit values are very close; assuming that thickness between substrate and the film has no decisive influence on the Ba/Sr ratio [13], and that BP_{DRX} is more accurate (for the R^2 fit value and for measuring the substitution of Ba into BST in a more significant volume than the BP_{EDS}). The BP_{DRX} is used to obtain x parameter vs APR and calculates the associated value of DR, E_g and RST into ISO colour-code lines corresponding to Figures 3a, 4a and 6a respectively. The maximum and minimum values of DR, E_g, and RST are obtained from the intersection of APR, and temperature ranges (375-435 °C), (435-495 °C) and (495-549 °C) and this are shown in Table 2.

Figure 2b the maximum peak of BP_{DRX} derivative, the applied power equilibrium ratio to obtain Ba/Sr = 50%/50% is reaching with PAR≈45/75 or 5/3.

Highest content zone >%Sr^{2+} (APR=0-45 W) >%Ba^{2+} (APR=45-120 W)		**Temperature ranges (°C)**					
		375-435		**435-495**		**495-549**	
		Max	**min**	**Max**	**Min**	**Max**	**min**
Deposition rate (nm/min)	**(Sr)**	2.53	1.84	2.63	1.84	2.43	1.74
	(Ba)	6.45	2.82	6.25	2.63	5.57	2.43
Eg (eV)	**(Sr)**	4.52	3.94	4.51	3.82	3.91	3.80
	(Ba)	4.52	3.89	4.49	3.82	4.39	3.79
RST ρ (Ω*cm)	**(Sr)**	0.03	0.03	0.84	0.03	1	0.09
	(Ba)	0.57	0.03	0.84	0.03	0.84	0.06

Table 2. Analysis of RD, Eg and RST maximum and minimum values, replicated with ISO-colour coded lines in APR and temperature intersection

Figure 2c (second derivative of BP_{DRX}) represents the stoichiometric difference related to Δ(Sr-Ba)/Δ(P_2-P_1) gradient. The positive gradient corresponds to the zone with Sr excess (ΔP_{Sr}≈45-0≈45) and the negative gradient to the zone with Ba excess (ΔP_{Ba}≈120-45≈75), The area under the curve (ΔP_{Sr}, y_{max}), defines the magnitude of Sr excess that reaches a maximum peak and decreases until Δ(Sr-Ba) = 0. Similarly, the negative gradient with an area under the curve (ΔP_{Ba}, y_{min}) is interpreted. The BP second derivative helps to understand the joint operation of the two magnetrons and deposit stages where Ba has a higher sputtering yield than that of Sr due to its higher ionic radius.

Preprints (www.preprints.org) | NOT PEER-REVIEWED | Posted: 9 October 2017 doi:10.20944/preprints201710.0043.v1

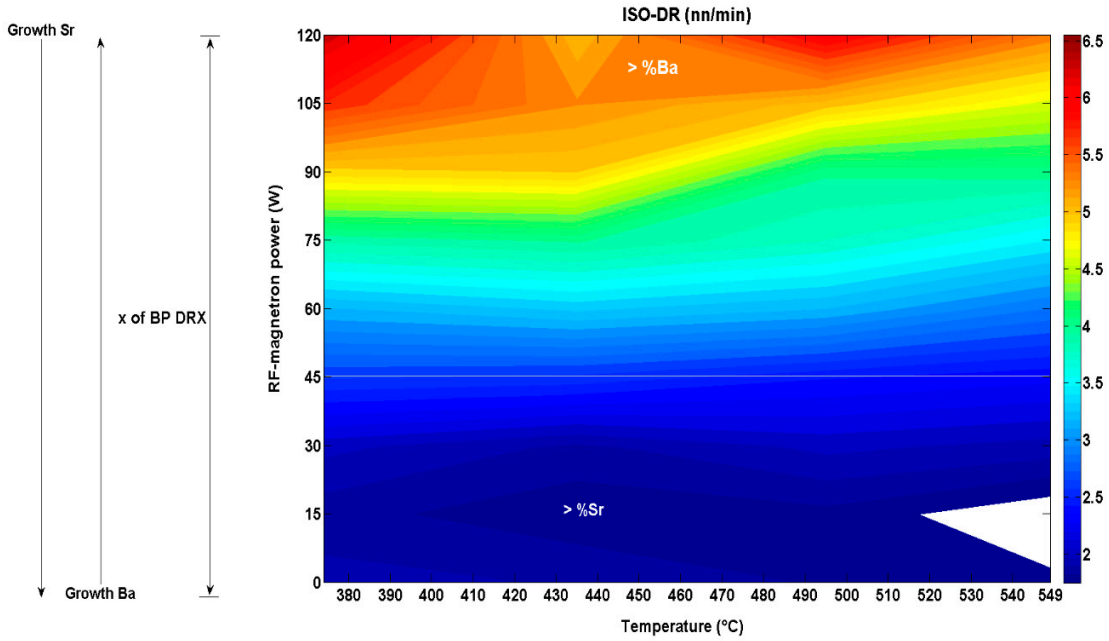

Figure 3a. ISO-DR lines with APR of 0-120 (W) and temperature range 375-549 °C.

Figure 3a represents DR projection values (dimensioned in the right column) by ISO colour-coded lines for APR and temperature ranges indicating that DR decrease when the temperature range and Sr content increase, particularly notorious when APR=45-120 W and temperature 435-549 °C zones. The highest DR values APR=105-120 W and <375 °C ranges. The temperature range of 375-460 °C shows an instability region by the transition from amorphous to the crystalline phase. The maximum and minimum values confirm this trend, see Table 2.

When the deposition temperature increases the DR profile decreases, this behaviour can be explained by ideal gases law (PV = nRT), where "n" is ionised argon atoms number, when deposition temperature increase the working pressure too, to keep it constant, the system decreases the reactive gas flow [20].

Preprints (www.preprints.org) | NOT PEER-REVIEWED | Posted: 9 October 2017 doi:10.20944/preprints201710.0043.v1

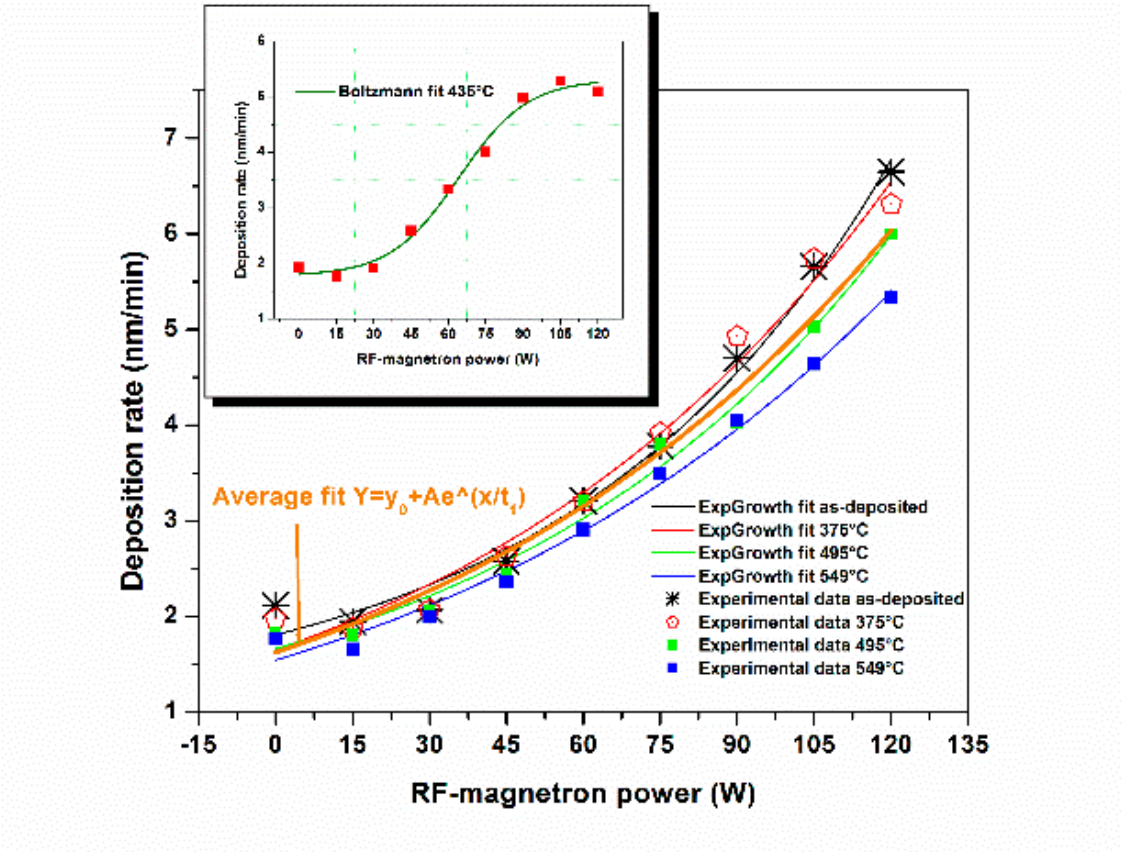

Figure 3b. DR for each temperature and fit with EG for as-deposited temperatures, 375 ° C, 495 ° C, 549 ° C, and average fit, the inset shows the ratio of deposit and the fit with the BP for the temperature of 435 °C.

Figure 3b shows DR for each temperature and fit with E_g for temperatures: as-deposited, 375, 495, 549 °C, whose equation is defined as:

$$Y = DR_0 + Ae^{P/t1}$$

Where: DR_0 is the deposition rate, A and t1 are constants and P are applied power.

In the average DR fit (discrete experimental data) the deposition ratio Ba/Sr≈3/1 corresponding to maximum and minimun points respectively.

The inset in figure 3b shows DR vs BP fit for 435°C. This behaviour can be explained due to target erosion rate (TER) may vary when the reactive gas supply is kept constant [20]. As will be seen, this temperature is critical in the transition from the amorphous to the crystalline phase.

Preprints (www.preprints.org) | NOT PEER-REVIEWED | Posted: 9 October 2017 doi:10.20944/preprints201710.0043.v1

Figure 4a represents E_g values projection (dimensioned in the right column) using ISO colour-coded lines for APR and temperature ranges. The maximum and minimum values obtained from ISO lines for E_g indicate a downward trend when temperature and Ba content increase (see Table 2), however, there is a transition zone with the highest E_g values in the power range 45-60 W and temperature 375-495 °C, because of these zones are transitions between the amorphous and crystalline phases, as shown in figure 4b and confirmed by XDR, in addition, the value of E_g can be affected by stoichiometric ratio Sr-rich and/or Ba-rich of the area where the transmission spectrum is taken.

The trend when "x" increases is according to [11,12,13, 22]. Comparing E_g between 375-495 °C and 45-75 W ranges, when the temperature increases the E_g too, this behaviour can be attributed to Ba content and the amorphous phase.

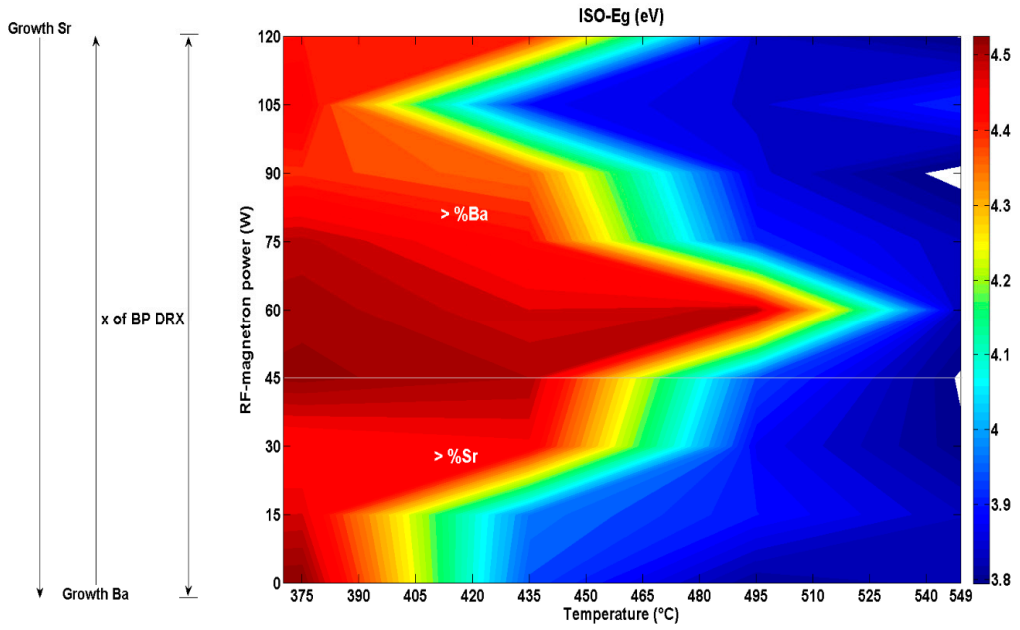

Figure 4a. ISO-E_g lines with APR of 0-120 (W) and temperature range of 370-549 °C.

Table 3 shows the applied power-temperature relationships related to the parameter "x" where the ISO-E_g lines (obtained into figure 4a values) replicate the E_g values and the "x" parameter of the bibliographic references [R] for amorphous and crystalline phases.

Preprints (www.preprints.org) | NOT PEER-REVIEWED | Posted: 9 October 2017 doi:10.20944/preprints201710.0043.v1

Amorphous phase		T (°C)	APR (W)	[R]	Crystalline phase		T (°C)	APR (W)	[R]
%x	E_g (eV)				%x	E_g (eV)			
80	4.18	495	65/55	[16]	80	3.8	>535	65/55	[16]
70	4.27	495	55/65	[25]	75	3.88-3.83	>535	60/60	[15]
70	4.58	<375	55/65	[17]	70	3.94	>535	55/65	[17]
65	4.39	475	52/68	[27]	50	3.96	495	45/75	[28]
50	4.2	465	45/75	[18]	60	3.81	549	50/70	[11]
50	4.75	<375	45/75	[14]	100	3.75	>549	120/0	[11]
					0	3.88	495	0/120	[11]

Table 3 Analysis to replicate E_g and parameter "x" values as a function of APR and temperature rate

Figure 4b shows E_g values for all samples (B0S120 to B120S0) and temperatures: as-deposited (50°C as reference), 375, 435, 495, and 549°C. The broken red lines represent the lowest and highest E_g values of the BST referenced in the literature and define the transition zone between the amorphous and crystalline phases. The solid line is the BP fit of the E_g average at each temperature. From the experimental data, E_g decreases when the temperature increases according to [14,15,17]. The results of XDR confirm that some samples of the temperatures 375, 435, 495, 549 °C have different crystallinity degrees and suggest the presence of both crystalline and amorphous phases, in addition to improvement in crystallinity with the increase of the temperature. The difference in amorphous and crystalline E_g values suggests that there may be band bending in the amorphous phase and decreasing with increasing temperature or crystallinity. The reduction in the E_g with increasing crystallinity indicates that the separation between the levels of the oxygen and titanium ions are influenced by a long-range order and crystal size. The role of electron-phonon interaction may be determinant in the optical properties of BST [17].

Preprints (www.preprints.org) | NOT PEER-REVIEWED | Posted: 9 October 2017 doi:10.20944/preprints201710.0043.v1

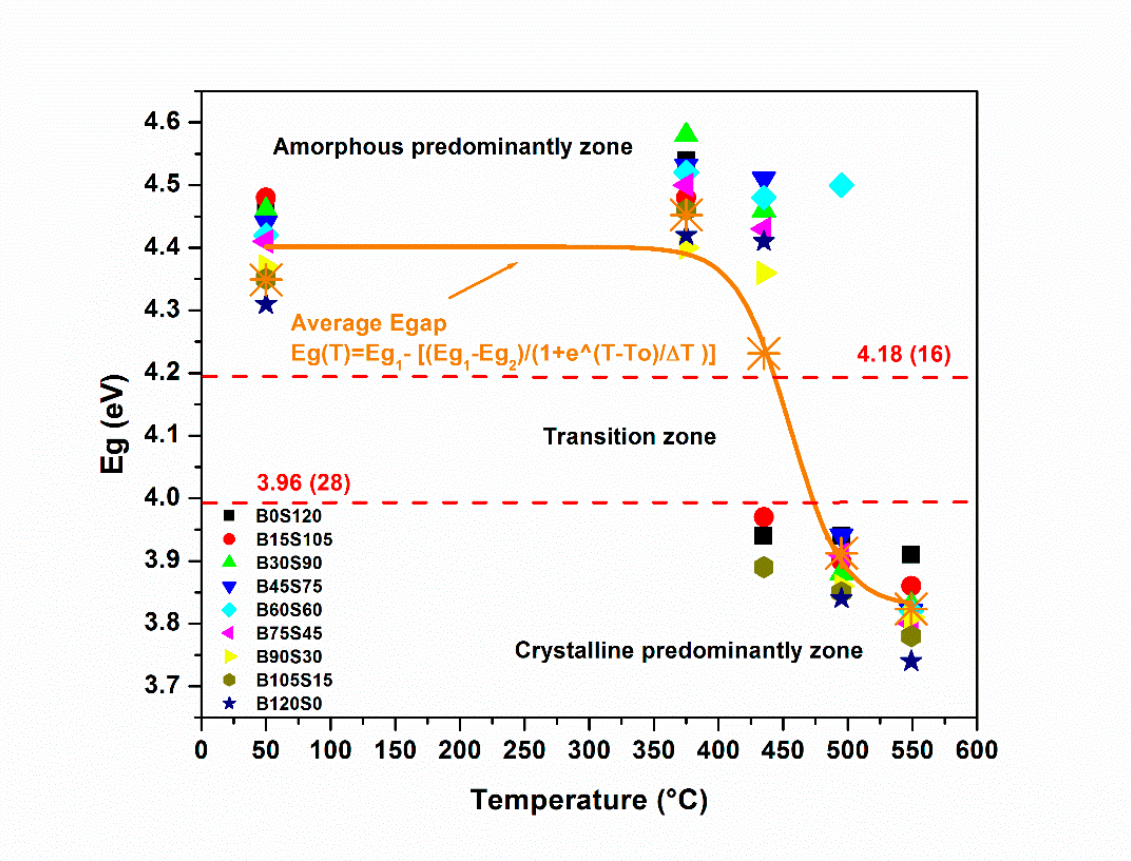

Figure 4b. E_g values, B0S120-B120S0 samples as a function of temperature, as-deposited samples have been plotted at 50 °C as the reference temperature.

Another possible reason for larger values of E_g in the amorphous phase is the existence of the density of states as explained by Davis and Mott [18]. The E_g values of this research work and the bibliography of Table 3 were found above some reported [22,23,24].

The authors explain these differences due to: a) the change in crystal structure [11], b) phase change [15], c) the increase in interatomic space due to excess volume and absence of long-range order in the lattice, in addition to the Burstein-Moss effect due to oxygen vacancies [14] d) the change in size of the microstructure [16], e) the presence of amorphous material and the effect of quantum size [25,26,28].

For the temperature of 549 °C, the XDR spectrum (not shown here) defines a polycrystalline film with cubic, tetragonal and orthorhombic phases. [13]. These results suggest that the crystalline structure through a transition state to achieve stability and that E_g values can decrease with higher deposit temperatures.

Preprints (www.preprints.org) | NOT PEER-REVIEWED | Posted: 9 October 2017 doi:10.20944/preprints201710.0043.v1

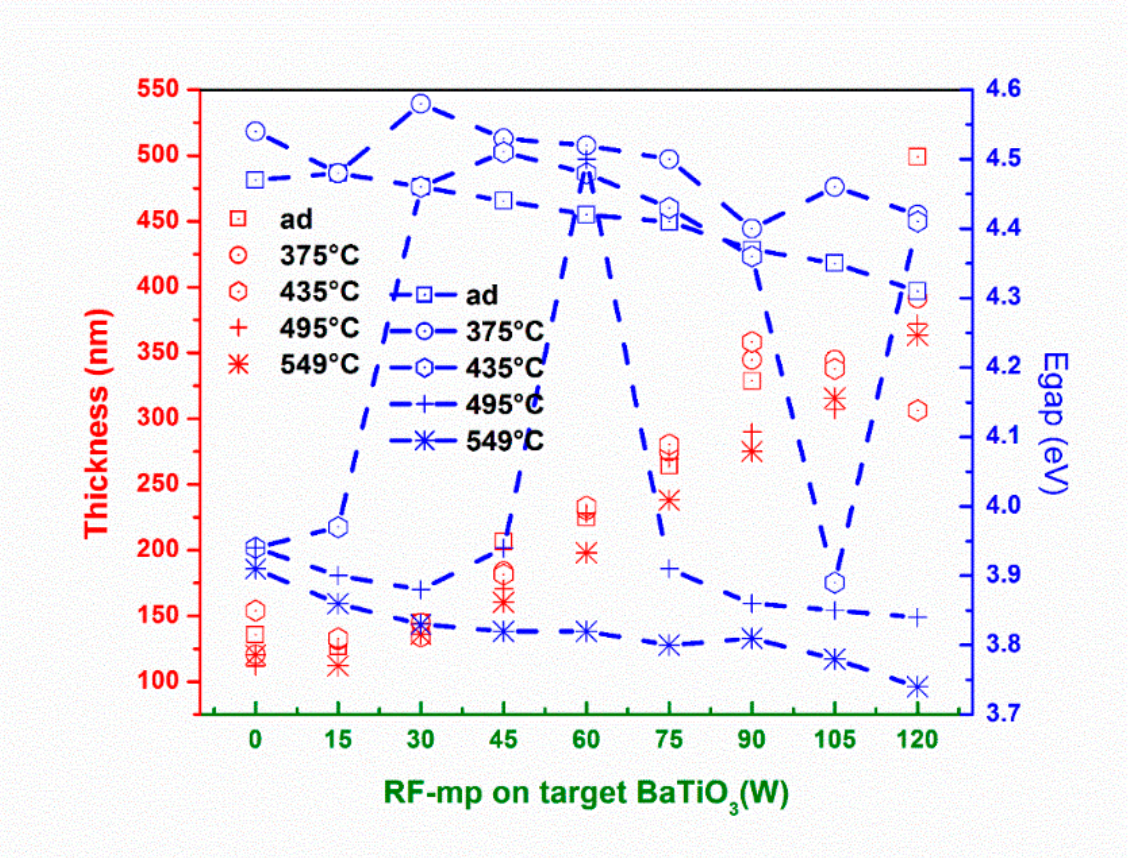

Figure 5. Thickness and E_g as a function of RF-mp.

In figure 5 comparing the E_g values (samples B0S120-B120S0, except B60S60) from the temperatures 495°C and 549°C, and taking into account the trends of the ISO lines DR, we can observe that the effect of film thickness has a slight effect on the E_g [12].

Figure 6a represents RST values projection (dimensioned in the right column) using ISO colour-code lines for APR and temperature ranges, the maximum and minimum values of RST are obtained (see table 2), which show a tendency to higher values of RST when the temperature and Sr content increase [14], particularly in the applied power zone 0-45 W and temperature 495-549 °C. White applied power and temperature ranges would indicate conductivity and the necessity of more samples to achieve complete the ISO-RST lines. Other authors report only lower resistivity with Sr increase [15,20].

Preprints (www.preprints.org) | NOT PEER-REVIEWED | Posted: 9 October 2017 doi:10.20944/preprints201710.0043.v1

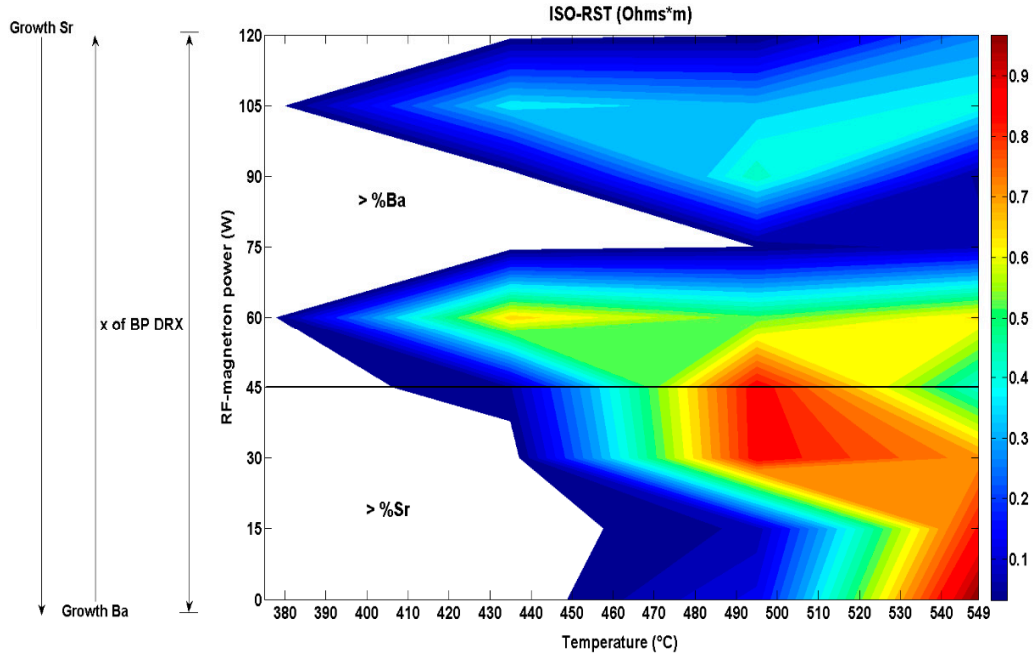

Figure 6a. ISO-RST lines with APR of 0-120 (W) and temperature range 375-549 °C.

Figure 6b shows RST values for all of the samples (B0S120 to B120S0) and, temperatures. The drawn profile of the S-shaped average RST, similar to BP, has been reported for compositions of “x” from 10 to 70 percent and temperatures from -150 to 150 °C [7]. The down-values of RST for all compositions by the effect of the temperature from as-deposited up to 375 °C coincides with the change from amorphous to a crystalline phase, and it is evident that at 375 °C there is a much more marked transition into phases.

Preprints (www.preprints.org) | NOT PEER-REVIEWED | Posted: 9 October 2017 doi:10.20944/preprints201710.0043.v1

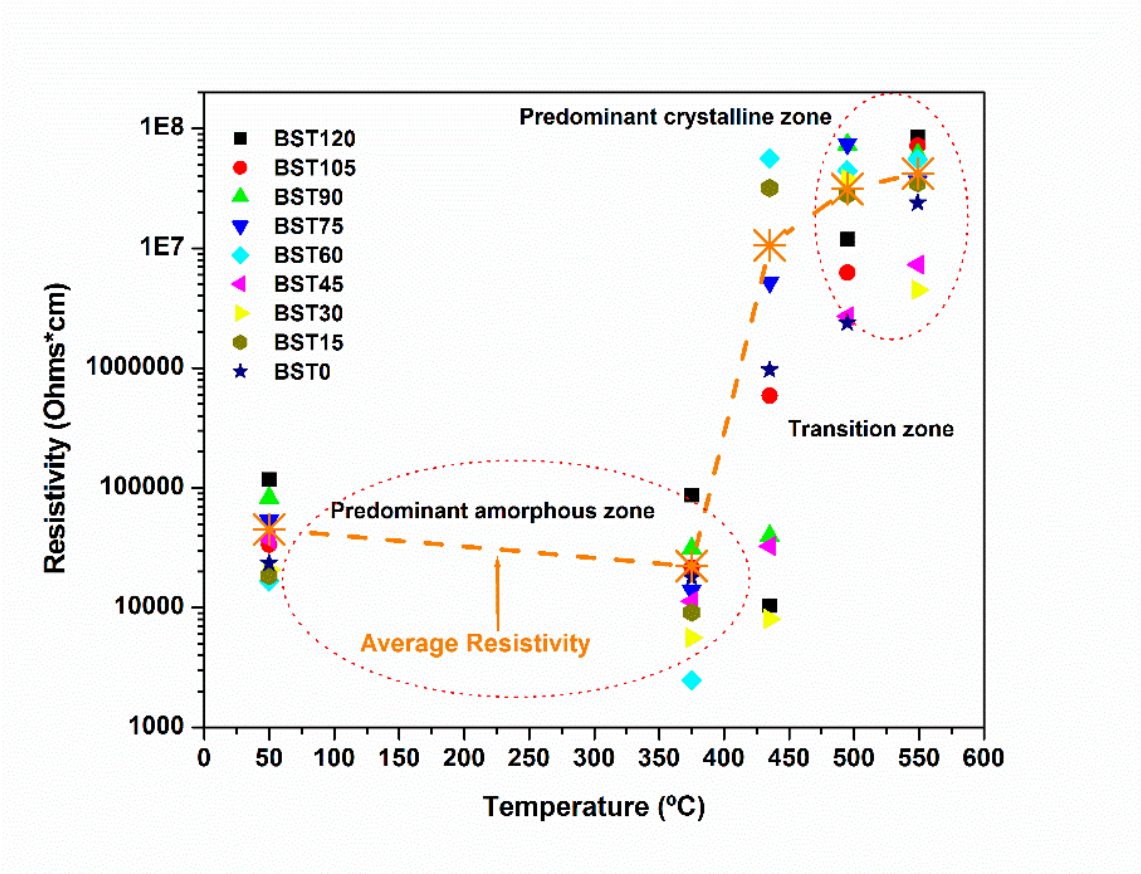

Figure 6b. RST values, samples of B0S120-B120S0 as a function of temperature, as-deposited samples have been plotted at 50 °C as the reference temperature.

4. Conclusions

The DR, E_g and RST analysis of the combined effect of applied power control parameters, in situ temperature and stoichiometric content, for thin films deposited by RF-co-sputtering allows a correct interpretation of the system and can make much more accurate the experimentation and control of material properties. This methodology can be applied when control parameters such as the work pressure and the Ar/O_2 ratio are variable. BP is present in the system as follows: "x" vs P for amorphous and crystalline phases, Eg vs T (°C) transition between amorphous and crystalline phase, E_g vs "x" for crystalline phase. The "S" shape of RST vs T (°C) can be analyzed in limits containing the BP for the transition from amorphous to the crystalline phase.

5. Acknowledgments

We are grateful for the technical support received during execution of this work from José Manuel Zavala Carrillo and Rolando Juárez Alvarez. JEM is also grateful to CONACyT for the financing of the Project “Recovery of matrix oil and density enhancement (API) of heavy and extra-heavy crude by in situ hydro-processing” (code 177007). JLFM contribution was supported by SIP-IPN Multidisciplinary Project 20170215, and by EDI and SIBE-IPN grants.
Instituto Politécnico Nacional.

References

[1] Bussmann-Holder, Annette. "The polarizability model for ferroelectricity in perovskite oxides." *Journal of Physics: Condensed Matter 24, no. 27 (2012): 273202.*

[2] Dubou Rdieu, Catherine, John Bruley, Thomas M. Arruda, Agham Posadas, Jean JordanSweet, Martin M. Frank, Eduard Cartier et al. "Switching of ferroelectric polarization in epitaxial $BaTiO_3$ films on silicon without a conducting bottom electrode." *Nature Nanotechnology 8, no. 10 (2013): 748-754.*

[3] J.C. Agar, S. Pandya, R. Xu, A.K. Yadav, Z. Liu, T. Angsten, S. Saremi, M. Asta, R. Ramesh, L.W. Martin, Frontiers in strain-engineered multifunctional ferroic materials, *MRS Commun. 6 (2016) 151-166.*

[4] Liu, S. J., Xu, C. Y., Zeng, X. B., Shi, J. Q., & Zhao, B. F. (2002). Preparation of (Ba0. 67Sr0. 33) TiO3 thin films for the dielectric bolometer mode of uncooled infrared focal plane arrays. *Physica status solidi (a), 194(1), 64-70.*

[5] Zapata-Navarro, A., Márquez-Herrera, A., Cruz-Jáuregui, M. P., & Calzada, M. L. (2005). Ferroelectric properties of barium strontium titanate thin films grown by RF co-sputtering. *Physica status solidi (c), 2(10), 3673-3676.*

[6] Márquez-Herrera, A., Hernández-Rodríguez, E., Cruz, M. P., Calzadilla-Amaya, O., Meléndez-Lira, M., Guillén-Rodríguez, J., & Zapata-Torres, M. (2010). Electrical properties of resistive switches based on Ba1-xSr xTiO3 thin films prepared by RF co-sputtering. *Revista mexicana de física, 56(5), 401-405.*

[7] C. Moure J, El titanato de bario como material semiconductor. Boletín de la Sociedad *Español de cerámica y vidrio, 18(6) 389-395.*

[8] Panda, B., Roy, A., Dhar, A., & Ray, S. K. (2007). Thickness and temperature dependent electrical characteristics of crystalline $Ba_xSr_{1-x}TiO_3$ thin films. *Journal of applied physics, 101(6), 064116.*

[9] Patil, D. R., Lokare, S. A., Devan, R. S., Chougule, S. S., Kanamadi, C. M., Kolekar, Y. D., & Chougule, B. K. (2007). Studies on electrical and dielectric properties of $Ba_{1-x}Sr_xTiO_3$. *Materials chemistry and physics, 104(2), 254-257.*

[10] Reséndiz-Muñoz J., Corona Rivera M., Fernández-Muñoz J.L., et al., Mathematical model Boltzmann's sigmoidal equation applicable to the setup of the RF-magnetron co-sputtering in thin films deposition of $Ba_XSr_{1-X}TiO3$. Accepted 12/05/2016. *Bulletin of Materials Science. (Ref.: Ms. No. BOMS-D-16-01560).*

[11] Wang, G. S., Zhang, Y. Y., Mao, C. L., Dong, X. L., & Chu, J. H. (2007). Composition dependence of structural and optical properties for sol-gel derived (100)-oriented $Ba_{1-x}Sr_xTiO_3$ thin films. *Applied Physics Letters, 91(6), 061104.*

[12] Leng, W. J., Yang, C. R., Zhang, J. H., Chen, H. W., Ji, H., Fu, C. L., & Liao, J. X. (2006). Structural and optical properties of $Ba_xSr_{1-x}TiO_3$ thin films on indium tin oxide/quartz substrates prepared by radio-frequency magnetron sputtering. *Journal of applied physics, 99(11), 114904.*

[13] Reséndiz-Muñoz, J., Fernández-Muñoz, J. L., Corona-Rivera, M. A., Zapata-Torres, M., Márquez-Herrera, A., Meléndez-Lira, M., & Zelaya-Ángel, O. (2017). Stoichiometry Calculation in BaxSr1−xTiO3 Solid Solution Thin Films, Prepared by RF Cosputtering, Using X-Ray Diffraction Peak Positions and Boltzmann Sigmoidal Modelling. *Journal of Nanomaterials, 2017.*

[14] Roy, S. C., Sharma, G. L., & Bhatnagar, M. C. (2007). Large blue shift in the optical band-gap of sol-gel derived $Ba_{0.5}Sr_{0.5}TiO_3$ thin films. *Solid state communications, 141(5), 243-247.*

[15] Železný, V., Chvostová, D., Pajasová, L., Jelínek, M., Kocourek, T., Daniš, S., & Valvoda, V. (2014). Temperature dependence of the optical properties of $Ba_{0.75}Sr_{0.25}TiO_3$ thin films. *Thin Solid Films, 571, 416-419.*

[16] Wang, J. , Huang, L., Xie, Y.-N., Hua, Q., Bai, L.-Y. Dongbei Daxue Xuebao. (2010). Effect of sputtering pressure on the optical properties of BST thin films. *Journal of Northeastern University*. *31 (2010), Issue SUPPL. 2, 68-70.*

[17] Singh, S. B., Sharma, H. B., Sarma, H. N. K., & Phanjoubam, S. (2008). Influence of crystallisation on the spectral features of nano-sized ferroelectric barium strontium titanate ($Ba_{0.7}Sr_{0.3}TiO_3$) thin films. *Physica B: Condensed Matter, 403(17), 2678-2683.*

[18] Saravanan, K. V., Sudheendran, K., Krishna, M. G., Raju, K. J., & Bhatnagar, A. K. (2006). Effect of process parameters and post-deposition annealing on the optical, structural and microwave dielectric properties of RF magnetron sputtered $(Ba_{0.5},Sr_{0.5})TiO_3$ thin films. *Vacuum, 81(3), 307-316.*

[19] Wang, S. F., Yang, H. C., Liu, C. F., & Bor, H. Y. Y. (2014). Characteristics of bilayer molybdenum films deposited using RF sputtering for back contact of thin film solar cells. *Advances in Materials Science and Engineering, 2014.*

[20] Berg, S., & Nyberg, T. (2005). Fundamental understanding and modeling of reactive sputtering processes. *Thin solid films, 476(2), 215-230.*

[21] Li, S., Yao, Y., Jia, Y., & Cui, Z. (2014). Phase formation and microstructure of $Ba_xSr_{1-x}TiO3$ ceramics prepared by direct current arc discharge plasma process. *Materials Letters, 123, 235-237.*

[22] Tian, H. Y., Chan, H. L. W., Choy, C. L., & No, K. (2003). The effects of composition gradients of $Ba_xSr_{1-x}TiO3$ thin films on their microstructures, dielectric and optical properties. *Materials Science and Engineering: B, 103(3), 246-252.*

 doi:10.20944/preprints201710.0043.v1

[23] Panda, B., Dhar, A., Nigam, G. D., Bhattacharya, D., & Ray, S. K. (1998). Optical properties of RF sputtered strontium substituted barium titanate thin films. *Thin Solid Films, 332(1), 46-49.*

[24] Pontes, F. M., Leite, E. R., Pontes, D. S. L., Longo, E., Santos, E. M. S., Mergulhao, S., & Varela, J. A. (2002). Ferroelectric and optical properties of $Ba_{0.8}Sr_{0.2}TiO_3$ thin film. *Journal of Applied Physics, 91(9), 5972-5978.*

[25] Xu, Z., Tanushi, Y., Suzuki, M., Wakushima, K., & Yokoyama, S. (2006). Optical properties of amorphous $Ba_{0.7}Sr_{0.3}TiO_3$ thin films obtained by metal organic decomposition technique. *Thin Solid Films, 515(4), 2326-2331.*

[26] Bao, D., Yang, H., Zhang, L., & Yao, X. (1998). Structure and Optical Properties of $SrTiO_3$ Thin Films Prepared by a Sol-Gel Technique. *Physica status solidi (a), 169(2), 227-233.*

[27] Lu, H., Pan, J. S., Chen, X. F., Zhu, W. G., & Tan, O. K. (2006). Influence of annealing temperature on the band structure of sol-gel $Ba_{0.65}Sr_{0.35}TiO_3$ thin films on n-type Si (100). *Applied physics letters, 88(13), 132907.*

[28] Tcheliebou, F., Ryu, H. S., Hong, C. K., Park, W. S., & Baik, S. (1997). On the microstructure and optical properties of $Ba_{0.5}Sr_{0.5}TiO_3$ films. *Thin Solid Films, 305(1-2), 30-34.*